THE JOURNAL OF
PHYSICAL CHEMISTRY
LETTERS
A JOURNAL OF THE AMERICAN CHEMICAL SOCIETY

Unveiling the Role of Termination Groups in Stabilizing MXenes in Contact with Water

Valentina Nesterova, Vladislav Korostelev, and Konstantin Klyukin*

Cite This: J. Phys. Chem. Lett. 2024, 15, 3698−3704

Read Online

ACCESS | Metrics & More | Article Recommendations | Supporting Information

ABSTRACT: MXenes are versatile 2D materials demonstrating outstanding electrochemical and physical properties, but their practical use is limited, because of fast degradation in an aqueous environment. To prevent the degradation of MXenes, it is essential to understand the atomistic details of the reaction and to identify active sites. In this letter, we provided a computational analysis of the degradation processes at the interface between MXene basal planes and water using enhanced sampling *ab initio* molecular dynamics simulations and symbolic regression analysis. Our results indicate that the reactivity of Ti sites toward the water attack reaction depends on both local coordination and chemical composition of the MXene surfaces. Decreasing the work function of the $Ti_3C_2T_x$ surfaces and avoiding Ti sites that are loosely anchored to the subsurface (e.g., O-coordinated) can improve surface stability. The developed computational framework can be further used to investigate other possible culprits of the degradation reaction, including the role of defects and edges.

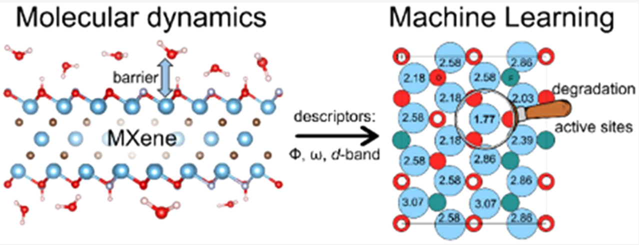

MXenes belong to the class of two-dimensional (2D) transition metal carbides or carbonitrides with the general formula of $M_{n+1}X_nT_x$ ($n = 1-4$), where M stands for a transition metal, X for carbon and/or nitrogen, and T for surface termination groups (e.g., −OH, −O, and − F). 2D MXene nanosheets are synthesized by the selective removal of metal atoms (e.g., Al) from precursor materials that belong to a large family of layered carbides/nitrides called MAX phases.[1,2] The wide range of possible compositions and rich surface chemistry distinguishes MXenes from other commonly studied 2D materials such as graphene and transition metal dichalcogenides.[3,4] In the past few years, experimental studies of the physical and chemical properties of various MXenes have revealed their great promise for a broad spectrum of applications including electrochemical energy storage,[3,5−8] flexible and transparent electronics,[9,10] chemical and biosensing applications,[11−13] water desalination and purification,[14,15] electromagnetic shielding,[16,17] and catalysis.[18−20]

Despite their intriguing performance, their low stability limits the practical applications of MXenes. Their 2D nanosheets tend to undergo rapid degradation in aqueous media or humid environments, resulting in the formation of their respective metal oxides.[21−26] Even the most stable and the most studied $Ti_3C_2T_x$ MXenes show notable degradation after being dispersed in water for a week.[21,27] While the lifespan of dried freestanding $Ti_3C_2T_x$-MXene layers can be extended even for years,[28] films of different compositions can degrade when stored at ambient conditions.[29] Recent studies have identified two major culprits causing the degradation of MXenes: water[30] and oxygen molecules.[31] The reported exponential decay in the rate of oxidation of MXenes exposed to a humid environment[31,32] suggests the existence of active sites catalyzing the oxidation reaction. While these sites are saturated, the reaction slows down. Several studies hypothesized that edges of MXenes are more prone to oxidative degradation,[31,33] while others suggested that degradation starts at the basal plane of MXenes and that the presence of defects should be considered a possible source of instability.[34] Since the conflicting opinions on the origin of material degradation can lead to different degradation prevention strategies, revealing the active sites catalyzing the degradation process is pivotal for the effective design and implementation of MXene-based materials.

Termination groups are exposed to the environment and can be one of the key factors determining the stability of MXenes. Although MXenes are known for their rich and tunable surface chemistry, the role of termination groups in degradation processes remains poorly understood. Moreover, the rich surface chemistry of MXenes represents a significant challenge for *ab initio*-based simulations due to a large combinatorial space of surface compositions. Therefore, most of the previous simulations were focused mainly on fully O-, OH-, or F-terminated MXene, which cannot be realized experimentally. Several computational studies quantified the role of termi-

Received: January 4, 2024
Revised: February 19, 2024
Accepted: February 21, 2024
Published: March 28, 2024

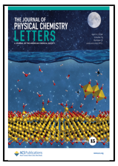

https://doi.org/10.1021/acs.jpclett.4c00045

nation groups in the stability of MXenes by employing *ab initio* thermodynamic analysis (i.e., by constructing Pourbaix diagrams[35,36] and calculating defect formation energies[37]). These studies indicated that O-terminated MXenes are the most stable, while the presence of hydroxyl and fluorine termination groups decreases the stability, promoting the formation of Ti vacancies.[37] More recent studies employing *ab initio* molecular dynamics (AIMD) simulations revealed spontaneous degradation of O-terminated surface MXenes surfaces (e.g., $Ti_3C_2O_2$[38,39] and V_2CO_2[40]) in contact with an aqueous environment. These works emphasize the need for advanced computational methods to evaluate the stability and understand the atomistic mechanism of MXene degradation.

In this computational study, we investigated the degradation reactions at the interface between $2\sqrt{3} \times 4$ surface cells of $Ti_3C_2T_x$ (T_x = OH, O, Cl, F, and their mixture) and aqueous solution (Figure S1), revealing sites that are the most prone for degradation reaction. (see SI for more details) To quantify the kinetic aspects of MXene stability in contact with water, we used AIMD simulations complemented with enhanced free energy sampling. These methods have been successfully used by us and others to study catalytic and degradation reaction mechanisms at solid−water interfaces.[41−47] To evaluate activation energy associated with Ti atoms oxidation at the MXene−water interfaces, we divided the trajectories obtained from the slow-growth method[48] into simulation windows separated by 0.1 Å and performed Blue-Moon sampling simulations,[49] collecting energy gradients acting on the Ti atom during at least 5 ps and further integrating the trajectory to get a free energy surface. The distance between Ti and C atoms was chosen as a reaction coordinate, and the simulations were carried out until the gradient acting on Ti reached zero.

As shown in Figure 1a, the release of Ti from the subsurface to the MXene surface is followed by the attack of the H_2O molecule, leading to the stabilization of the Ti−OH complex above the termination groups. After Ti is exposed to the solution, it reacts with two more water molecules, forming an octahedral hydroxide complex attached to the MXene surface (Figure S2). We further calculated the activation energies (E_A) of the first step of the described reaction by integrating the energy gradients along the reaction coordinate. It is possible for the process to occur spontaneously at the O-terminated Ti_3C_2 surface[38] due to a low E_A of 0.28 eV, as shown in Figure 1b. However, the release of the second Ti atom on the same surface was found to be much less favorable, with an E_A of 1.04 eV (see Figure S3). These results are in qualitative agreement with recent simulations conducted for V_2CO_2.[50] We attribute this behavior to changes in electrostatic potential associated with the formation of a Ti(V)−OH dipole, as explained in more detail below.

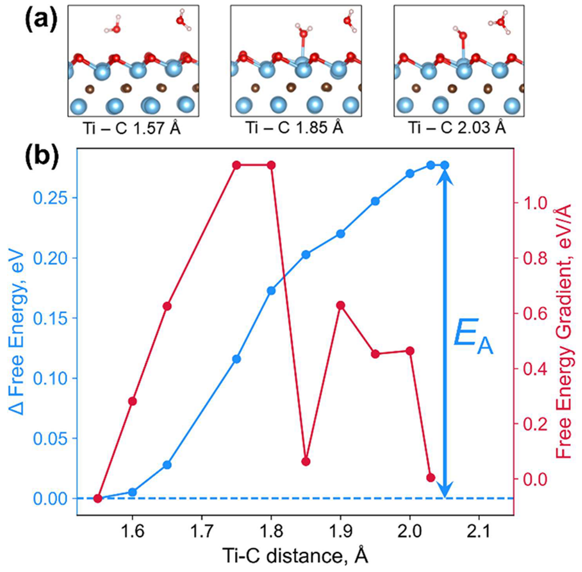

Figure 1. (a) Representative snapshots of the AIMD trajectory demonstrating Ti release from the $Ti_3C_2O_2$ surface and its reaction with water. (b) Free energy gradients (right-hand scale) and free energy landscape (left-hand scale) along the reaction coordinate (distance between Ti atom and C atoms), where E_A is the activation energy of the Ti release.

We further calculated E_A for Ti sites at various $Ti_3C_2T_x$ surfaces, including O-, OH-, and F- and their mixed terminations (see Table S2). Our simulations revealed that E_A varies from 0.28 eV for the O-terminated surface to more than 3.9 eV for the OH-terminated surface, depending on the global composition of termination groups and the local coordination of Ti sites. For example, E_A for the 3O-coordinated Ti atom increases from 0.28 eV at the O-terminated $Ti_3C_2O_2$ to 1.58 eV for $Ti_3C_2\,(OH)_{0.67}O_{1.33}$ and becomes 2.15 eV for $Ti_3C_2\,(OH)_{1.33}O_{0.67}$. Notably, the kinetics of Ti oxidation and defect formation energy of the Ti vacancy for various $Ti_3C_2T_x$ surfaces demonstrate the opposite trends (see Figure 2). Although the formation of the Ti vacancy is the least energetically favorable at the $Ti_3C_2O_2$ surface (vacancy formation energy of 8.39 eV in agreement with previous studies[37]), the small E_A of 0.28 eV indicates that the O-terminated surface of $Ti_3C_2O_2$ is intrinsically unstable. Based on these results, we propose that the degradation of MXene surfaces is a kinetically limited process, and increasing the barrier (E_A) associated with the initial step of the degradation reaction (i.e., metal ion release above the surface) can be considered as an indicator of MXene stability.

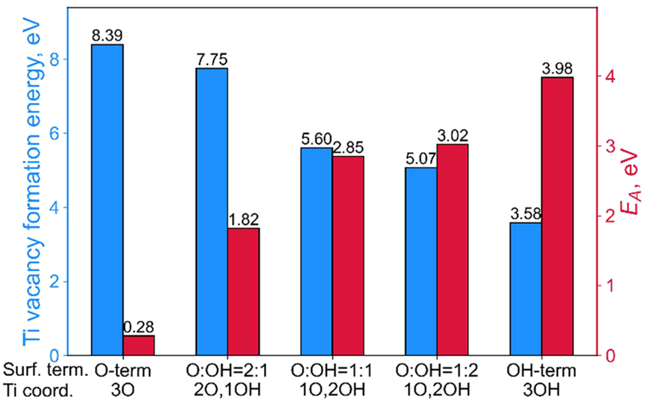

Figure 2. Ti atom vacancy formation energy (left-hand scale) and activation energy E_A of Ti release and oxidation in contact with water (right-hand scale) for $Ti_3C_2T_x$ with different terminations. The most commonly occurring coordination of Ti is shown for each surface.

Activation energy (E_A) values vary greatly depending on both the local coordination of Ti and the surface composition, making the identification of Ti sites prone to oxidation for each specific surface composition rather challenging. In particular, the systematic exploration of the stability for the vast space of MXene surface compositions is limited by time-consuming

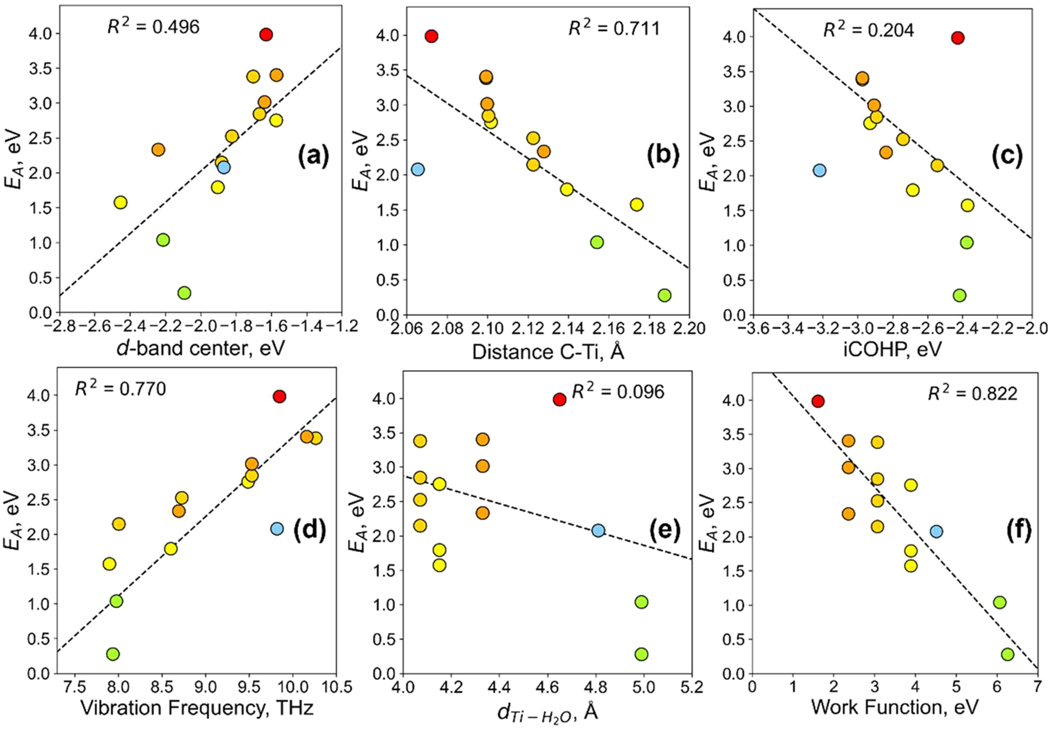

Figure 3. Correlations between activation energies of Ti release (E_A) and descriptive properties of $Ti_3C_2T_x$ surfaces: (a) *d*-band center of Ti, (b) average distance from Ti to three adjacent C atoms, (c) integrated COHP of Ti, (d) out-of-plane vibrational frequencies of Ti, (e) an average distance between the outer layer of Ti and O from water molecules, and (f) work function of the considered surface. Colors represent various terminations: green, O; yellow, 1OH:2O; gold, 1OH:1O; orange, 2OH:1O; red, OH; and blue, F.

AIMD simulations. Establishing relations between E_A values and descriptive properties of MXene surfaces can facilitate the identification of active sites for the degradation reaction and accelerate the design of stable MXene chemistries. Below, we search for simple properties of $Ti_3C_2T_x$ MXene surfaces associated with the kinetics of Ti atom oxidation in contact with water. We consider both local traits of $Ti_3C_2T_x$ surfaces describing the specific Ti site, such as *d*-band center, C−Ti distance, and out-of-plane Ti vibration frequency, and global properties of the surface, such as an average distance from Ti to water molecules and work function. The obtained correlations between the selected properties of MXene surfaces and activation energies are shown in Figure 3a−f and in Figure S4.

We first explored the local properties associated with specific Ti sites at $Ti_3C_2T_x$ surfaces. Figure 3a shows the correlation between the E_A and *d*-band center of the Ti site, which characterizes *d*-orbital occupancy and is commonly applied in predicting the reactivity of transition metals.[51−54] We propose that the *d*-band characterizes both the propensity of Ti for the oxidation reaction (i.e., dissociation of water) and the strength of Ti bonds with the surface. Our simulations demonstrated that the lower values of the Ti *d*-band center indicate lower E_A values, which is supported by the correlation coefficient R^2 = 0.496. The bond strength between C and Ti atoms is another critical local feature affecting Ti activity toward the water attack reaction. In Figure 3b, we used an average distance between Ti and three neighboring C atoms as a geometry-based indicator of bond strength. The shorter C−Ti bonds imply a stronger connection of Ti to the $Ti_3C_2T_x$ surface resulting in a strong negative correlation between average C−Ti interatomic distance and E_A. In Figure 3c, we also correlated the E_A values associated with each Ti site with an average integrated Crystal Orbital Hamilton Population (iCOHP) between Ti and neighboring C atoms, which indicates the bond strength between the adjacent atoms and has been successfully used as a descriptor of catalytic activity[55] and adsorption energy[56,57] in the literature. Negative iCOHP values suggest stronger bonds, indicating greater resistance to bond breaking processes like oxidation. Therefore, a more negative iCOHP between Ti and C implies a stronger bond, leading to higher E_A values of reactions involving bond disruption. The positive correlation between activation energies and Ti vibration frequencies (Figure 3d) was found to be the strongest among the studied local descriptors. The lower frequency corresponds to softer out-of-plane Ti vibrations, leading to a less steep energy surface for Ti release. In this work, we used the vibration frequencies of Ti along the *c*-direction, which can be calculated by displacing the single Ti atom and fixing the rest of the atoms in the unit cell as implemented in the finite differences approach.[58] This method is very computationally efficient, and the calculated frequencies demonstrate good agreement with a more accurate projection of the phonon band on Ti atoms (Figure S5). These findings highlight the important role of dynamic features, such as vibration frequencies and phonon modes, as promising descriptors associated with not only the conductivity of small ions,[59−61] but also with surface reactivity and stability.

We further explored correlations between E_A and global properties of $Ti_3C_2T_x$ surfaces such as an average distance between Ti and water molecules and work function. We initially hypothesized that a short distance between outer Ti atoms and the first water layer (i.e., "wettability" of the $Ti_3C_2T_x$ surface) could promote a water attack reaction. We calculated the first peak position d_{Ti-H2O} of the radial distribution function (RDF) between water molecules and

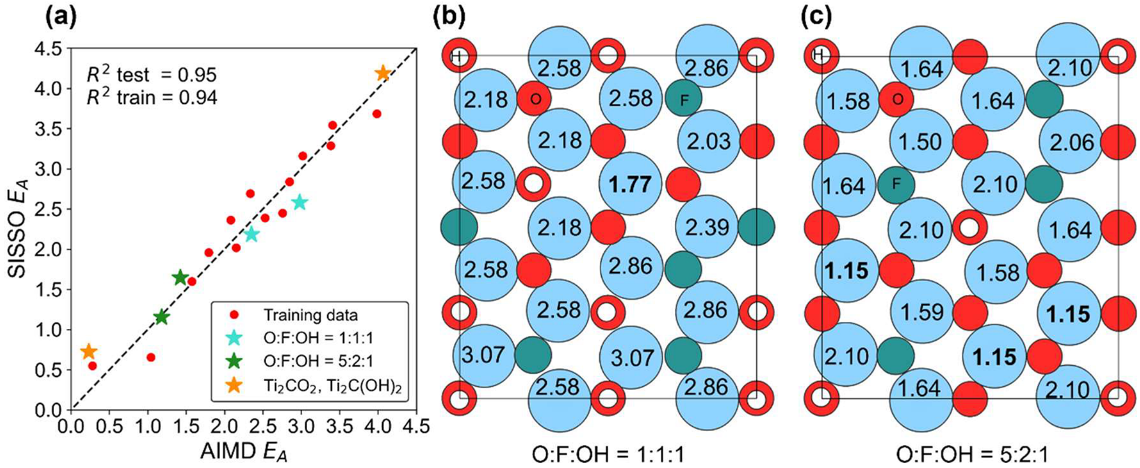

Figure 4. (a) Comparison of AIMD-calculated energy barriers (AIMD E_A) and energy barriers predicted with the SISSO machine learning model (SISSO E_A). Predicted E_A for $Ti_3C_2T_x$ surfaces of different composition: O:OH:F = 1:1:1 (b) and O:F:OH = 5:2:1 (c). Bold labels indicate the active sites of the degradation reaction (i.e., the lowest E_A).

the outer Ti layer (Figure S6), which indicates the average distance between Ti and the O atoms belonging to the first layer of water. However, our simulations revealed a relatively weak correlation between d_{Ti-H2O} and E_A (Figure 3e), suggesting that the proximity of water to Ti is not a determining factor of the reaction rate. On the other hand, AIMD simulations revealed a strong negative correlation (R^2 = 0.822) between E_A and the work function of $Ti_3C_2T_x$ surfaces (Figure 3f). This property describes the position of the Fermi level in relation to the vacuum level and is associated with the electrostatic potential of the surfaces. Several previous studies correlated work functions to the catalytic activity of metallic surfaces.[62−64] However, the effect of the work function on surface stability has not been explored. In this work, we discovered that the stability of $Ti_3C_2T_x$ surfaces is linked to their work function: $Ti_3C_2T_x$ surfaces with lower work functions generally demonstrate higher stability (Figure 3f). As discussed earlier, we also observed that the subsequent oxidation and release of Ti atoms raised E_A for future reactions, hindering the degradation. We now attribute this behavior to the alteration in work function (6.26 eV vs 6.07 eV after the release of Ti) due to the formation of a Ti−OH dipole on the surface of $Ti_3C_2O_2$.

After establishing the structure−stability relationships, we utilized the selected descriptive properties to predict the stability of $Ti_3C_2T_x$ with various compositions of termination groups and to identify sites catalyzing the degradation reaction. In order to build a predictive model and identify the best combination of descriptors, we employed symbolic regression machine learning algorithms as implemented in SISSO code.[65] The best performing model obtained after dimensionality reduction (see Figures S7 and S8) relies on two descriptive properties:

$$E_A = -0.45\Phi + 0.03\omega^2 + 1.43 \qquad (1)$$

where E_A is the predicted activation energy of Ti release, Φ is the work function (eV), and ω stands for the vibrational frequency of Ti along the c direction (THz). Our results suggest that decreasing the work function of the $Ti_3C_2T_x$ surface and avoiding Ti sites that are loosely anchored to the subsurface (as characterized by soft phonon modes) can improve the surface stability. These surface properties can be rapidly calculated for MXene of any selected composition and, therefore, can be used for computational screening and the selection of surface chemistries impeding degradation reactions.

Figure 4 presents the performance of the derived analytical equation in predicting E_A for several surface compositions previously unseen by the model. The testing data set includes complex surfaces terminated with a mixture of O, OH, and F groups and Ti_2CT_x compounds. The predicted and calculated values of E_A for the testing data set, along with associated descriptors, are provided in Table S3. As seen in Figure 4a, the constructed analytical formula exhibits excellent performance in predicting E_A with a low mean absolute error of 0.24 eV and a high R^2 score (R^2 = 0.95) on the testing data set. The model can be used for the identification of sites prone to degradation reactions at the surface of any composition without performing time-consuming AIMD calculations. Figure 4b,c illustrates the application of our model to identify sites catalyzing the degradation reaction at surfaces with mixed termination: O:F:OH compositions of 1:1:1 and 5:2:1, where the last one was obtained experimentally.[66] These preliminary results indicated that the O-coordinated Ti sites have the lowest E_A values (i.e., 1.77 and 1.15 eV) for Ti release and further oxidation in contact with H_2O molecules, suggesting that avoiding these sites can impede the initial steps of the degradation reaction.

In summary, our simulations demonstrated that the kinetics of the initial steps of the degradation reaction play a key role in determining surface stability. For the first time, the role of termination groups in the stability of MXenes in contact with water was quantified using enhanced sampling *ab initio* molecular dynamics. According to our calculations, Ti reactivity toward the water attack reaction depends on both the local coordination of Ti sites and the chemical composition of the MXene surface. Our results also indicate that surface transformation occurring during the degradation reaction (e.g., release of Ti atoms) can modify local and global traits of the surface, significantly affecting the degradation reaction rate on the adjacent sites. We found strong correlations of the E_A barrier associated with the initial steps of degradation reaction starting at the basal plane of $Ti_{n+1}C_nT_x$ (n = 1, 2) MXenes with local properties of Ti sites, such as the d-band center, out-of-plane vibrations, and average C−Ti distance, and with the work function, characterizing the electrostatic potential of the surface. Using machine learning algorithms, we combined physics-based descriptors into the analytical formula, allowing us to predict E_A for the reaction of Ti with H_2O molecules at $Ti_{n+1}C_nT_x$ (n = 1, 2) surfaces with different terminations (T_x = O, OH, F, and their mixture) and to identify the active sites of degradation reaction based on simple DFT calculations. The computational framework developed in the present work can be further used to investigate other possible culprits of the degradation reaction, including the role of defects[37] and edges,[27,33,67] and would shed light on the instability of MXenes beyond $Ti_3C_2T_x$.

■ ASSOCIATED CONTENT

Data Availability Statement

Simulation cells and the data sets with descriptors obtained and used in this study are openly available at 10.6084/m9.figshare.25236772.v1.

Supporting Information

The Supporting Information is available free of charge at https://pubs.acs.org/doi/10.1021/acs.jpclett.4c00045.

> Detailed description of static DFT calculations, parameters of *ab initio* molecular dynamics, $Ti_3C_2T_x$ descriptors calculations, and data analytics model (PDF)

■ AUTHOR INFORMATION

Corresponding Author

Konstantin Klyukin − *Department of Mechanical and Materials Engineering, Auburn University, Auburn, Alabama 36849, United States;* orcid.org/0000-0001-8325-8725; Email: klyukin@auburn.edu

Authors

Valentina Nesterova − *Department of Mechanical and Materials Engineering, Auburn University, Auburn, Alabama 36849, United States;* orcid.org/0009-0002-6585-3138

Vladislav Korostelev − *Department of Mechanical and Materials Engineering, Auburn University, Auburn, Alabama 36849, United States;* orcid.org/0000-0003-2380-5170

Complete contact information is available at: https://pubs.acs.org/10.1021/acs.jpclett.4c00045

Notes

The authors declare no competing financial interest.

■ ACKNOWLEDGMENTS

We acknowledge funding support from the National Science Foundation (DMREF-2324156). The authors acknowledge the Stampede2 at Texas Advanced Computing Center (TACC) at The University of Texas at Austin for providing computational resources through allocation MAT230066 from the Advanced Cyberinfrastructure Coordination Ecosystem: Services & Support (ACCESS).[68]

■ REFERENCES

(1) Cao, F.; Zhang, Y.; Wang, H.; Khan, K.; Tareen, A. K.; Qian, W.; Zhang, H.; Ågren, H. Recent Advances in Oxidation Stable Chemistry of 2D MXenes. *Adv. Mater.* **2022**, *34* (13), 2107554.

(2) Naguib, M.; Kurtoglu, M.; Presser, V.; Lu, J.; Niu, J.; Heon, M.; Hultman, L.; Gogotsi, Y.; Barsoum, M. W. Two-Dimensional Nanocrystals Produced by Exfoliation of Ti_3AlC_2. *Adv. Mater.* **2011**, *23* (37), 4248−4253.

(3) Anasori, B.; Lukatskaya, M. R.; Gogotsi, Y. 2D Metal Carbides and Nitrides (MXenes) for Energy Storage. *Nat. Rev. Mater.* **2017**, *2* (2), 16098.

(4) Naguib, M.; Mochalin, V. N.; Barsoum, M. W.; Gogotsi, Y. 25th Anniversary Article: MXenes: A New Family of Two-Dimensional Materials. *Adv. Mater.* **2014**, *26* (7), 992−1005.

(5) Lukatskaya, M. R.; Mashtalir, O.; Ren, C. E.; Dall'Agnese, Y.; Rozier, P.; Taberna, P. L.; Naguib, M.; Simon, P.; Barsoum, M. W.; Gogotsi, Y. Cation Intercalation and High Volumetric Capacitance of Two-Dimensional Titanium Carbide. *Science* **2013**, *341* (6153), 1502−1505.

(6) Lukatskaya, M. R.; Kota, S.; Lin, Z.; Zhao, M.-Q.; Shpigel, N.; Levi, M. D.; Halim, J.; Taberna, P.-L.; Barsoum, M. W.; Simon, P.; Gogotsi, Y. Ultra-High-Rate Pseudocapacitive Energy Storage in Two-Dimensional Transition Metal Carbides. *Nat. Energy* **2017**, *2*, 17105.

(7) Naguib, M.; Halim, J.; Lu, J.; Cook, K. M.; Hultman, L.; Gogotsi, Y.; Barsoum, M. W. New Two-Dimensional Niobium and Vanadium Carbides as Promising Materials for Li-Ion Batteries. *J. Am. Chem. Soc.* **2013**, *135* (43), 15966−15969.

(8) Li, C.; Wang, S.; Wang, X.; Bai, W.; Sun, H.; Pan, F.; Chi, Y.; Wang, Z. High-Temperature Supercapacitors Based on MXene with Ultrahigh Volumetric Capacitance. *ACS Mater. Lett.* **2023**, *5* (8), 2084−2095.

(9) Ling, Z.; Ren, C. E.; Zhao, M.-Q.; Yang, J.; Giammarco, J. M.; Qiu, J.; Barsoum, M. W.; Gogotsi, Y. Flexible and Conductive MXene Films and Nanocomposites with High Capacitance. *Proc. Natl. Acad. Sci. U.S.A.* **2014**, *111*, 16676.

(10) Zhang, C. J.; Anasori, B.; Seral-Ascaso, A.; Park, S.-H.; McEvoy, N.; Shmeliov, A.; Duesberg, G. S.; Coleman, J. N.; Gogotsi, Y.; Nicolosi, V. Transparent, Flexible, and Conductive 2D Titanium Carbide (MXene) Films with High Volumetric Capacitance. *Adv. Mater.* **2017**, *29*, 1702678.

(11) Wang, F.; Yang, C.; Duan, C.; Xiao, D.; Tang, Y.; Zhu, J. An Organ-Like Titanium Carbide Material (MXene) with Multilayer Structure Encapsulating Hemoglobin for a Mediator-Free Biosensor. *J. Electrochem. Soc.* **2015**, *162* (1), B16−B21.

(12) Lee, E.; VahidMohammadi, A.; Prorok, B. C.; Yoon, Y. S.; Beidaghi, M.; Kim, D.-J. Room Temperature Gas Sensing of Two-Dimensional Titanium Carbide (MXene). *ACS Appl. Mater. Interfaces* **2017**, *9* (42), 37184−37190.

(13) Wu, G.; Du, H.; Pakravan, K.; Kim, W.; Cha, Y. L.; Beidaghi, M.; Zhang, X.; Pan, X.; Kim, D.-J. Wearable Room-Temperature Ethanol Sensor Based on Ti3C2Tx/Polypyrrole Functionalized Face Mask for Drunk Driving Monitoring. *Carbon* **2024**, *216*, 118565.

(14) Peng, Q.; Guo, J.; Zhang, Q.; Xiang, J.; Liu, B.; Zhou, A.; Liu, R.; Tian, Y. Unique Lead Adsorption Behavior of Activated Hydroxyl Group in Two-Dimensional Titanium Carbide. *J. Am. Chem. Soc.* **2014**, *136* (11), 4113−4116.

(15) Mashtalir, O.; Cook, K. M.; Mochalin, V. N.; Crowe, M.; Barsoum, M. W.; Gogotsi, Y. Dye Adsorption and Decomposition on Two-Dimensional Titanium Carbide in Aqueous Media. *J. Mater. Chem. A* **2014**, *2* (35), 14334−14338.

(16) Shahzad, F.; Alhabeb, M.; Hatter, C. B.; Anasori, B.; Man Hong, S.; Koo, C. M.; Gogotsi, Y. Electromagnetic Interference Shielding with 2D Transition Metal Carbides (MXenes). *Science* **2016**, *353* (6304), 1137−1140.

(17) Han, M.; Yin, X.; Wu, H.; Hou, Z.; Song, C.; Li, X.; Zhang, L.; Cheng, L. Ti3C2MXenes with Modified Surface for High-Performance Electromagnetic Absorption and Shielding in the X-Band. *ACS Appl. Mater. Interfaces* **2016**, *8* (32), 21011−21019.

(18) Xie, X.; Chen, S.; Ding, W.; Nie, Y.; Wei, Z. An Extraordinarily Stable Catalyst: Pt NPs Supported on Two-Dimensional $Ti_3C_2X_2$ (X = OH, F) Nanosheets for Oxygen Reduction Reaction. *Chem. Commun.* **2013**, *49* (86), 10112−10114.

(19) Seh, Z. W.; Fredrickson, K. D.; Anasori, B.; Kibsgaard, J.; Strickler, A. L.; Lukatskaya, M. R.; Gogotsi, Y.; Jaramillo, T. F.; Vojvodic, A. Two-Dimensional Molybdenum Carbide (MXene) as an

Efficient Electrocatalyst for Hydrogen Evolution. *ACS Energy Lett.* **2016**, *1* (3), 589−594.

(20) Ling, C.; Shi, L.; Ouyang, Y.; Chen, Q.; Wang, J. Transition Metal-Promoted V_2CO_2 (MXenes): A New and Highly Active Catalyst for Hydrogen Evolution Reaction. *Adv. Sci.* **2016**, *3* (11), 1600180.

(21) Doo, S.; Chae, A.; Kim, D.; Oh, T.; Ko, T. Y.; Kim, S. J.; Koh, D.-Y.; Koo, C. M. Mechanism and Kinetics of Oxidation Reaction of Aqueous Ti $_3$ C $_2$ T $_x$ Suspensions at Different pHs and Temperatures. *ACS Appl. Mater. Interfaces* **2021**, *13* (19), 22855−22865.

(22) Bhat, A.; Anwer, S.; Bhat, K. S.; Mohideen, M. I. H.; Liao, K.; Qurashi, A. Prospects Challenges and Stability of 2D MXenes for Clean Energy Conversion and Storage Applications. *Npj 2D Mater. Appl.* **2021**, *5* (1), 1−21.

(23) Huang, S.; Mochalin, V. N. Combination of High pH and an Antioxidant Improves Chemical Stability of Two-Dimensional Transition-Metal Carbides and Carbonitrides (MXenes) in Aqueous Colloidal Solutions. *Inorg. Chem.* **2022**, *61* (26), 9877−9887.

(24) Soomro, R. A.; Zhang, P.; Fan, B.; Wei, Y.; Xu, B. Progression in the Oxidation Stability of MXenes. *Nano-Micro Lett.* **2023**, *15* (1), 108.

(25) Athavale, S.; Micci-Barreca, S.; Arole, K.; Kotasthane, V.; Blivin, J.; Cao, H.; Lutkenhaus, J. L.; Radovic, M.; Green, M. J. Advances in the Chemical Stabilization of MXenes. *Langmuir* **2023**, *39* (3), 918−928.

(26) Athavale, S.; Micci-Barreca, S. A.; Arole, K.; Kotasthane, V.; Lutkenhaus, J. L.; Radovic, M.; Green, M. J. Effect of Terminal Groups on the Degradation Stability of $Ti_3C_2T_z$ MXenes. *Nanoscale* **2023**, *15* (30), 12567−12573.

(27) Zhao, X.; Vashisth, A.; Blivin, J. W.; Tan, Z.; Holta, D. E.; Kotasthane, V.; Shah, S. A.; Habib, T.; Liu, S.; Lutkenhaus, J. L.; Radovic, M.; Green, M. J. pH, Nanosheet Concentration, and Antioxidant Affect the Oxidation of $Ti_3C_2T_x$ and Ti_2CT_x MXene Dispersions. *Adv. Mater. Interfaces* **2020**, *7* (20), 2000845.

(28) Lee, A.; Shekhirev, M.; Anayee, M.; Gogotsi, Y. Multi-Year Study of Environmental Stability of $Ti_3C_2T_x$ MXene Films. *ArXiv*, 2023, DOI: 10.48550/arXiv.2312.11679.

(29) VahidMohammadi, A.; Mojtabavi, M.; Caffrey, N. M.; Wanunu, M.; Beidaghi, M. Assembling 2D MXenes into Highly Stable Pseudocapacitive Electrodes with High Power and Energy Densities. *Adv. Mater.* **2019**, *31* (8), 1806931.

(30) Huang, S.; Mochalin, V. N. Hydrolysis of 2D Transition-Metal Carbides (MXenes) in Colloidal Solutions. *Inorg. Chem.* **2019**, *58* (3), 1958−1966.

(31) Zhang, C. J.; Pinilla, S.; McEvoy, N.; Cullen, C. P.; Anasori, B.; Long, E.; Park, S.-H.; Seral-Ascaso, A.; Shmeliov, A.; Krishnan, D.; Morant, C.; Liu, X.; Duesberg, G. S.; Gogotsi, Y.; Nicolosi, V. Oxidation Stability of Colloidal Two-Dimensional Titanium Carbides (MXenes). *Chem. Mater.* **2017**, *29* (11), 4848−4856.

(32) Lipatov, A.; Alhabeb, M.; Lukatskaya, M. R.; Boson, A.; Gogotsi, Y.; Sinitskii, A. Effect of Synthesis on Quality, Electronic Properties and Environmental Stability of Individual Monolayer Ti_3C_2 MXene Flakes. *Adv. Electron. Mater.* **2016**, *2* (12), 1600255.

(33) Natu, V.; Hart, J. L.; Sokol, M.; Chiang, H.; Taheri, M. L.; Barsoum, M. W. Edge Capping of 2D-MXene Sheets with Polyanionic Salts To Mitigate Oxidation in Aqueous Colloidal Suspensions. *Angew. Chem.* **2019**, *131* (36), 12785−12790.

(34) Xia, F.; Lao, J.; Yu, R.; Sang, X.; Luo, J.; Li, Y.; Wu, J. Ambient Oxidation of Ti3C2MXene Initialized by Atomic Defects. *Nanoscale* **2019**, *11* (48), 23330−23337.

(35) López, M.; Exner, K. S.; Viñes, F.; Illas, F. Computational Pourbaix Diagrams for MXenes: A Key Ingredient toward Proper Theoretical Electrocatalytic Studies. *Adv. Theory Simul.* **2023**, *6* (10), 2200217.

(36) Gao, G.; O'Mullane, A. P.; Du, A. 2D MXenes: A New Family of Promising Catalysts for the Hydrogen Evolution Reaction. *ACS Catal.* **2017**, *7* (1), 494−500.

(37) Sang, X.; Xie, Y.; Lin, M.-W.; Alhabeb, M.; Van Aken, K. L.; Gogotsi, Y.; Kent, P. R. C.; Xiao, K.; Unocic, R. R. Atomic Defects in Monolayer Titanium Carbide ($Ti_3C_2T_x$) MXene. *ACS Nano* **2016**, *10* (10), 9193−9200.

(38) Wu, T.; Kent, P. R. C.; Gogotsi, Y.; Jiang, D. How Water Attacks MXene. *Chem. Mater.* **2022**, *34* (11), 4975−4982.

(39) Song, H.; Jiang, D. First Principles Insights into Stability of Defected MXenes in Water. *Nanoscale* **2023**, *15*, 16010.

(40) Hou, P.; Tian, Y.; Xie, Y.; Du, F.; Chen, G.; Vojvodic, A.; Wu, J.; Meng, X. Unraveling the Oxidation Behaviors of MXenes in Aqueous Systems by Active-Learning-Potential Molecular-Dynamics Simulation. *Angew. Chem.* **2023**, *135* (32), No. e202304205.

(41) Klyukin, K.; Rosso, K. M.; Alexandrov, V. Iron Dissolution from Goethite (α-FeOOH) Surfaces in Water by Ab Initio Enhanced Free-Energy Simulations. *J. Phys. Chem. C* **2018**, *122* (28), 16086−16091.

(42) Intan, N. N.; Pfaendtner, J. Role of Surface Features on the Initial Dissolution of $CH_3NH_3PbI_3$ Perovskite in Liquid Water: An Ab Initio Molecular Dynamics Study. *ACS Nano* **2023**, *17* (22), 22371−22387.

(43) Klyukin, K.; Zagalskaya, A.; Alexandrov, V. Role of Dissolution Intermediates in Promoting Oxygen Evolution Reaction at RuO_2 (110) Surface. *J. Phys. Chem. C* **2019**, *123* (36), 22151−22157.

(44) Leung, K. First-Principles Modeling of Mn(II) Migration above and Dissolution from $Li_xMn_2O_4$ (001) Surfaces. *Chem. Mater.* **2017**, *29* (6), 2550−2562.

(45) Benedek, R.; Thackeray, M. M.; Low, J.; Bučko, T. Simulation of Aqueous Dissolution of Lithium Manganate Spinel from First Principles. *J. Phys. Chem. C* **2012**, *116* (6), 4050−4059.

(46) Chaudhary, P.; Zagalskaya, A.; Over, H.; Alexandrov, V. Strain-Dependent Activity-Stability Relations in RuO_2 and IrO_2 Oxygen Evolution Catalysts. *ChemElectroChem.* **2024**, *11* (1), No. e202300659.

(47) Sharma, S.; Zagalskaya, A.; Weitzner, S. E.; Eggart, L.; Cho, S.; Hsu, T.; Chen, X.; Varley, J. B.; Alexandrov, V.; Orme, C. A.; Pham, T. A.; Wood, B. C. Metal Dissolution from First Principles: Potential-Dependent Kinetics and Charge Transfer. *Electrochim. Acta* **2023**, *437*, 141443.

(48) Jarzynski, C. Nonequilibrium Equality for Free Energy Differences. *Phys. Rev. Lett.* **1997**, *78* (14), 2690−2693.

(49) Carter, E. A.; Ciccotti, G.; Hynes, J. T.; Kapral, R. Constrained Reaction Coordinate Dynamics for the Simulation of Rare Events. *Chem. Phys. Lett.* **1989**, *156* (5), 472−477.

(50) Hou, P.; Tian, Y.; Xie, Y.; Du, F.; Chen, G.; Vojvodic, A.; Wu, J.; Meng, X. Unraveling the Oxidation Behaviors of MXenes in Aqueous Systems by Active-Learning-Potential Molecular-Dynamics Simulation. *Angew. Chem.* **2023**, *135* (32), No. e202304205.

(51) Xin, H.; Vojvodic, A.; Voss, J.; Nørskov, J. K.; Abild-Pedersen, F. Effects of *d*-Band Shape on the Surface Reactivity of Transition-Metal Alloys. *Phys. Rev. B* **2014**, *89* (11), 115114.

(52) Jiao, S.; Fu, X.; Huang, H. Descriptors for the Evaluation of Electrocatalytic Reactions: *d*-Band Theory and Beyond. *Adv. Funct. Mater.* **2022**, *32* (4), 2107651.

(53) Liu, X.; Zhang, Y.; Wang, W.; Chen, Y.; Xiao, W.; Liu, T.; Zhong, Z.; Luo, Z.; Ding, Z.; Zhang, Z. Transition Metal and N Doping on AlP Monolayers for Bifunctional Oxygen Electrocatalysts: Density Functional Theory Study Assisted by Machine Learning Description. *ACS Appl. Mater. Interfaces* **2022**, *14* (1), 1249−1259.

(54) Deng, T.; Cen, C.; Shen, H.; Wang, S.; Guo, J.; Cai, S.; Deng, M. Atom-Pair Catalysts Supported by N-Doped Graphene for the Nitrogen Reduction Reaction: *d*-Band Center-Based Descriptor. *J. Phys. Chem. Lett.* **2020**, *11* (15), 6320−6329.

(55) Zeng, Z.; Nong, W.; Li, Y.; Wang, C. Universal-Descriptors-Guided Design of Single Atom Catalysts toward Oxidation of Li_2S in Lithium-Sulfur Batteries. *Adv. Sci.* **2021**, *8* (23), 2102809.

(56) Gong, L.; Wang, X.; Zheng, T.; Liu, J.; Wang, J.; Yang, Y.-C.; Zhang, J.; Han, X.; Zhang, L.; Xia, Z. Catalytic Mechanism and Design Principle of Coordinately Unsaturated Single Metal Atom-Doped Covalent Triazine Frameworks with High Activity and Selectivity for CO_2 Electroreduction. *J. Mater. Chem. A* **2021**, *9* (6), 3555−3566.

(57) Fung, V.; Wu, Z.; Jiang, D. New Bonding Model of Radical Adsorbate on Lattice Oxygen of Perovskites. *J. Phys. Chem. Lett.* **2018**, *9* (21), 6321−6325.

(58) Gonze, X.; Lee, C. Dynamical Matrices, Born Effective Charges, Dielectric Permittivity Tensors, and Interatomic Force Constants from Density-Functional Perturbation Theory. *Phys. Rev. B* **1997**, *55* (16), 10355−10368.

(59) Muy, S.; Schlem, R.; Shao-Horn, Y.; Zeier, W. G. Phonon-Ion Interactions: Designing Ion Mobility Based on Lattice Dynamics. *Adv. Energy Mater.* **2021**, *11* (15), 2002787.

(60) Korostelev, V.; Wagner, J.; Klyukin, K. Simple Local Environment Descriptors for Accurate Prediction of Hydrogen Absorption and Migration in Metal Alloys. *J. Mater. Chem. A* **2023**, *11* (43), 23576−23588.

(61) Muy, S.; Voss, J.; Schlem, R.; Koerver, R.; Sedlmaier, S. J.; Maglia, F.; Lamp, P.; Zeier, W. G.; Shao-Horn, Y. High-Throughput Screening of Solid-State Li-Ion Conductors Using Lattice-Dynamics Descriptors. *iScience* **2019**, *16*, 270−282.

(62) Shen, X.; Pan, Y.; Liu, B.; Yang, J.; Zeng, J.; Peng, Z. More Accurate Depiction of Adsorption Energy on Transition Metals Using Work Function as One Additional Descriptor. *Phys. Chem. Chem. Phys.* **2017**, *19* (20), 12628−12632.

(63) Zeradjanin, A. R.; Vimalanandan, A.; Polymeros, G.; Topalov, A. A.; Mayrhofer, K. J. J.; Rohwerder, M. Balanced Work Function as a Driver for Facile Hydrogen Evolution Reaction - Comprehension and Experimental Assessment of Interfacial Catalytic Descriptor. *Phys. Chem. Chem. Phys.* **2017**, *19* (26), 17019−17027.

(64) Wang, X.; Ye, S.; Hu, W.; Sharman, E.; Liu, R.; Liu, Y.; Luo, Y.; Jiang, J. Electric Dipole Descriptor for Machine Learning Prediction of Catalyst Surface-Molecular Adsorbate Interactions. *J. Am. Chem. Soc.* **2020**, *142* (17), 7737−7743.

(65) Ouyang, R.; Curtarolo, S.; Ahmetcik, E.; Scheffler, M.; Ghiringhelli, L. M. SISSO: A Compressed-Sensing Method for Identifying the Best Low-Dimensional Descriptor in an Immensity of Offered Candidates. *Phys. Rev. Mater.* **2018**, *2* (8), 083802.

(66) Hope, M. A.; Forse, A. C.; Griffith, K. J.; Lukatskaya, M. R.; Ghidiu, M.; Gogotsi, Y.; Grey, C. P. NMR Reveals the Surface Functionalisation of Ti 3 C 2 MXene. *Phys. Chem. Chem. Phys.* **2016**, *18* (7), 5099−5102.

(67) Zhang, C. J.; Pinilla, S.; McEvoy, N.; Cullen, C. P.; Anasori, B.; Long, E.; Park, S.-H.; Seral-Ascaso, A.; Shmeliov, A.; Krishnan, D.; Morant, C.; Liu, X.; Duesberg, G. S.; Gogotsi, Y.; Nicolosi, V. Oxidation Stability of Colloidal Two-Dimensional Titanium Carbides (MXenes). *Chem. Mater.* **2017**, *29* (11), 4848−4856.

(68) Boerner, T. J.; Deems, S.; Furlani, T. R.; Knuth, S. L.; Towns, J. ACCESS: Advancing Innovation: NSF's Advanced Cyberinfrastructure Coordination Ecosystem: Services & Support. In *Practice and Experience in Advanced Research Computing*; PEARC '23; Association for Computing Machinery: New York, NY, USA, 2023; pp 173−176, DOI: 10.1145/3569951.3597559.